LANGMUIR

pubs.acs.org/Langmuir Article

Eco-friendly Approach for Creation of Resonant Silicon Nanoparticle Colloids

Marina Karsakova, Nadezhda Shchedrina, Artur Karamyants, Ekaterina Ponkratova, Galina Odintsova,* and Dmitry Zuev*

Cite This: *Langmuir* 2023, 39, 204–210 Read Online

ACCESS | Metrics & More | Article Recommendations | Supporting Information

ABSTRACT: The commercial application of Mie-resonant nanophotonic technologies currently used in various laboratory studies, from biosensing to quantum optics, appears to be challenging. Development of colloidal-based fabrication approaches is a solution to face the issue. In our research, we studied the fabrication of resonant Si nanoparticle (NP) arrays on a surface with controlled wettability. First, we use nanosecond (ns) laser ablation in water and subsequent density gradient separation to obtain colloids of resonant spherical crystalline silicon NPs with a low polydispersity index. Then, the same industrial ns laser is applied to create a wetting gradient on the steel substrate to initiate a self-assembly of the NPs deposited by drop casting. Thus, we use a single commercial ns laser for producing both the NPs and the hydrophilic wetting gradient. We apply an easily operating size separation technique and only nontoxic media. This research contributes to the large-scale fabrication of various optical devices based on resonant high-refractive index nanostructures by ecologically friendly self-assembly techniques.

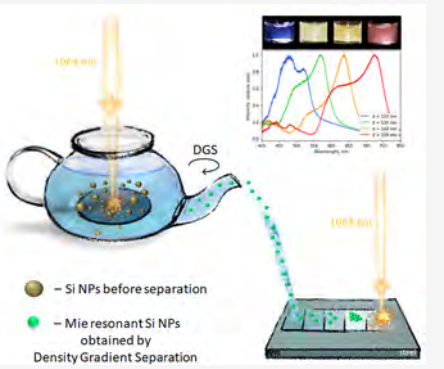

INTRODUCTION

In Mie-resonant nanophotonics, high refractive index (dielectric) nanosized elements with inherent electric and magnetic resonances provide enhanced scattering and low energy dissipation into heat. They possess strong nonlinear optical properties and are compatible with semiconductor device technologies.[1] Thus, these materials can be applied for sensing,[2−4] quantum technologies,[5] imaging,[6] flexible displays,[7] and high-performance optical devices.[8] On the other hand, a broader implementation of nanophotonic systems consisting of high-refractive index materials in everyday life requires a development of simple methods for a scalable production of resonant nanoparticles (NPs) with a proper geometric configuration as well as physical and chemical structure control.[9]

There are currently numerous methods for fabrication of dielectric nanostuctures, including lithography, dewetting, or some chemical methods.[10] However, despite the high productivity of chemical and dewetting methods, repeatability, and high resolution of lithography, a further development of fabrication techniques requires an eco-friendly approach and some solutions for large-scale production. One of the promising fabrication methods is self-assembling NPs over a substrate, which is usually conducted from the liquid phase.[11−16] An important step for adapting this approach to the fabrication of resonant high-refractive index nanostructures is producing colloidal solutions.

To create Mie-resonant dielectric NP colloids, various methods used polydisperse solution synthesis and its subsequent separation on narrow-sized inks. The most common method for the fabrication of wide-sized NP colloids is disproportionation. It implies high-temperature annealing of silicon monoxide with a subsequent etching.[17−19] This approach requires heating to 1500 °C in a nitrogen atmosphere and subsequent etching in hydrofluoric acid. Despite the advantages of the above technique, it has some issues with non-spherical NPs,[17] multi-stage processing, and environmental friendliness.[19] Femtosecond (fs) laser ablation of a bulk high-refractive index target in a liquid is an alternative approach to disproportionation.[20] In this approach, the narrow-sized distribution of NPs in the laser-generated colloid can hardly be achieved by a simple variation of laser ablation parameters. Therefore, the subsequent NP separation is required to obtain inks of Mie-resonant NPs of the specified size/color. Thus, for further development of the techniques for NP fabrication and separation, it is important to turn to using non-toxic media as well as to study the self-assembly option for the NPs from the fabricated inks.

Received: September 1, 2022
Revised: December 7, 2022
Published: December 21, 2022

https://doi.org/10.1021/acs.langmuir.2c02382
Langmuir 2023, 39, 204−210

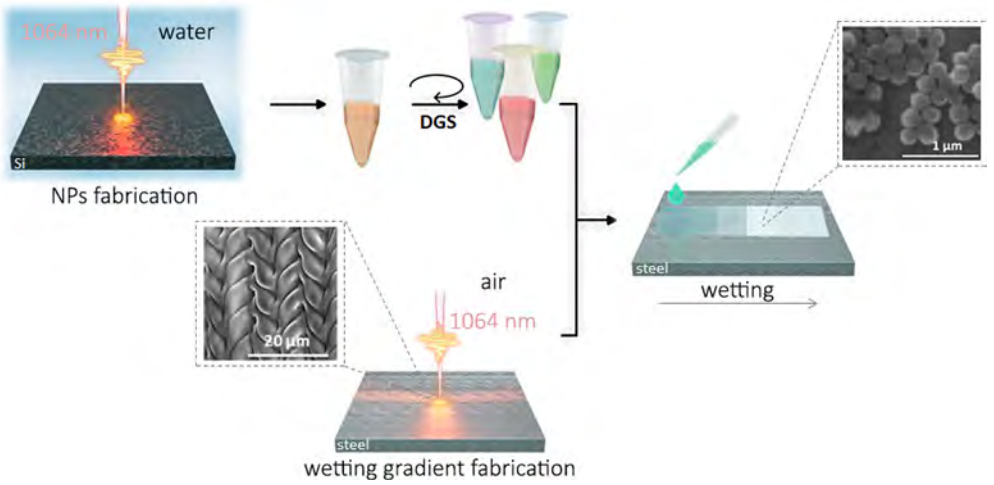

Figure 1. Overall experiment scheme: production of Si NP colloid solutions, steel laser structuring, and Si NP self-assembling on a steel substrate.

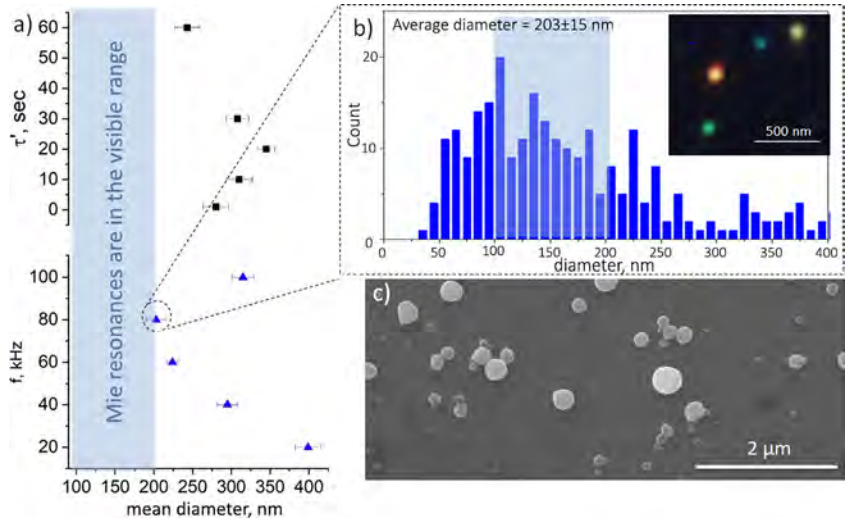

Figure 2. Optimization of the laser ablation conditions: (a) mean diameters of Si NPs, (b) size distribution diagram and DF image of the solution created via the selected regime, and (c) SEM image of the solution.

In view of the above, we develop an environmentally friendly method for producing Mie-resonant Si NP colloidal solutions followed by self-assembly. It implies Si NP size separation using the density gradient with a further controlled distribution over the surface with a hydrophilic wetting gradient for self-assembly (Figure 1).

In our research, we apply a single commercial nanosecond (ns) laser for producing both the NPs and the wetting gradient. We apply solely non-toxic media, such as water and sucrose water solution, for both Si NP colloid preparation and NP size distribution.

RESULTS AND DISCUSSION

Laser Fabrication of Si NPs. In this study, NPs are generated by pulsed laser ablation in a liquid (LAL), which allows for control of the NP properties using wavelength, pulse duration, frequency, pulse energy, and other laser radiation parameters.[21] In addition, the size of NPs can be controlled by varying the duration of the target exposure to laser irradiation or fragmenting the existing particles. NPs are formed as a result of the condensation of the plasma cloud produced by laser irradiation of a solid target. The process of NP generation includes two stages. First, a plasma cloud is formed; a cavitation bubble emerges and then collapses; a colloidal solution is formed; and there is interaction with the successive laser pulses. During the second stage, as a result of liquid convection, the synthesized particles fall into the laser spot region and can be fragmented.[21] Producing resonant NP colloids using a fs laser has been studied and discussed in detail.[22−24] Although a fs laser provides a more efficient ablation, it is the ns pulse duration that is superior in terms of fabrication productivity. Indeed, during ns laser ablation, the material output is much higher.[25]

The inherent nature of the ns laser interaction with the solid-state volume involves the subsequent heating and melting processes during the pulse, as opposed to the interaction with the electron system in the case of the fs pulse.[26] Moreover, during ns laser fabrication of colloids, the additional fragmentation process within pulse duration can take place. The laser fragmentation is a process of a size reduction of particles in a solution under the laser-assisted treatment of NP colloids. In such a process, laser radiation is focused in a colloid volume. The particles absorb the laser energy in a laser focal spot and are split into smaller pieces (fragmented) as a

https://doi.org/10.1021/acs.langmuir.2c02382
Langmuir 2023, 39, 204−210

result of the combination of photothermal evaporation and Coulomb explosion. For fragmentation of large sub-micrometer particles, both picosecond (ps)/fs and ns lasers can work effectively. However, in the case of the ns laser irradiation, the duration of the pulse is long enough: the pulse still lasts when the ablation/evaporation, thermal diffusion, and resolidification processes start on time.[27] Therefore, the ns laser pulse itself provides additional heating of the nanobubbles created around particles during the ablation process. Such nanobubbles create an atmosphere around irradiated NPs, facilitating evaporation processes and affecting agglomeration/fragmentation processes.[28] During the interaction of fs laser radiation with the target surface, thermo-induced nanobubbles are formed, which screen the target area. On the other hand, with the ns laser irradiation, the same laser pulse causes an additional NP fragmentation during the bubble−pulse interaction.[28] This, in turn, can be used for extra adjustment of the NP size distribution. For fs laser irradiation, the amount of material removed from the target can be increased by fluence enhancement; however, in this case, nonlinear effects of self-focusing and multiphoton absorption can take place.[28] Therefore, in our study, the ns laser pulses are chosen for fabrication resonant NP colloids. Our experiments were intended to generate Si NPs with average diameters of 100−200 nm in deionized (DI) water by laser ablation of the silicon target. Such sizes of the Si NPs make it possible to observe Mie resonances in the visible range.[29] For this purpose, as the first step of the experiments, we assessed the optimal parameters of the laser exposure duration and the pulse repetition rate. A commercial ytterbium fiber laser system (1.064 μm for 20 ns, Minimarker 2) is applied to scan the bulk Si surface immersed in deionized water (see Figure S1 of the Supporting Information). The scan pattern of the laser beam consists of non-overlapping spots with the distance of 350 μm. In the experiments, we used the laser fluence F of 4.38 J/cm^2. This fluence value is slightly higher than the Si ablation threshold in water to minimize the cavitation effects.

The results of the experiments are presented in Figure 2a. The laser processing parameters for each experiment are given in Tables 1 and 2 of the Supporting Information. We revealed that the change of the laser exposure duration τ' from 1 to 20 s leads to increasing the Si NP mean diameters. In turn, the successive increase of τ' to 60 s provides their decrease. Presumably, when the exposure duration is above 20 s, the fragmentation of the laser-synthesized particles occurs simultaneously with their generation. For the further experiments, the laser exposure duration τ' of 10 s was selected, because in this case, the ratio of the particle number/size distribution is close to 100−200 nm (see Figure S2 of the Supporting Information). An increase in the laser pulse repetition rate f from 20 to 80 kHz leads to the reduction of the Si NP mean diameters (see Figure 2a) to 100−200 nm. The repetition rate rising leads to a decrease in the concentration of the NPs and widening of the size distribution (see Figure S3 of the Supporting Information). This effect can result from the cavitation occurring in the laser spot area and an additional NP fragmentation. Thus, the optimal laser ablation parameters were determined as f = 80 kHz, F = 4.38 J/cm^2, τ = 20 ns, and τ' = 10 s, which provide the generation of Si NPs with the maximum size distribution in the range of 100−200 nm (Figure 2c).

Density Gradient Separation. Because a narrow size distribution of NPs is hard to achieve during the fabrication via pulsed laser ablation in liquid, the sucrose density gradient method (DGM) was chosen for the post-synthesis Si NP size control.[30] In DGM, a colloidal solution sample is placed on the top of a specially prepared density gradient, where the density increases from the top to the bottom. With this approach, the NPs of various sizes and shapes have different viscous resistance. This results in a difference in the sedimentation coefficients and, as a consequence, the sedimentation rates for each particle when a specified centrifugal force is applied. Upon centrifugation, the NPs of a certain size range are collected from the different layers of the solution based on their sizes/shapes. In our case, the density gradient was created by carefully layering six sucrose solutions of different concentrations with their densities varying from 1.13 to 1.35 g/cm^3.

Under the centrifugal forces (4000 rpm for 5 min), the particles precipitated through the gradient column in separate zones, with each zone consisting of the particles specified by their size and sedimentation rate. The layers were extracted from the top of the colorful gradient and replaced in different vials. Figure 3 shows that size-separated solutions demonstrate distinctive colors from blue to red as a result of Mie scattering of Si NPs in the visible range.

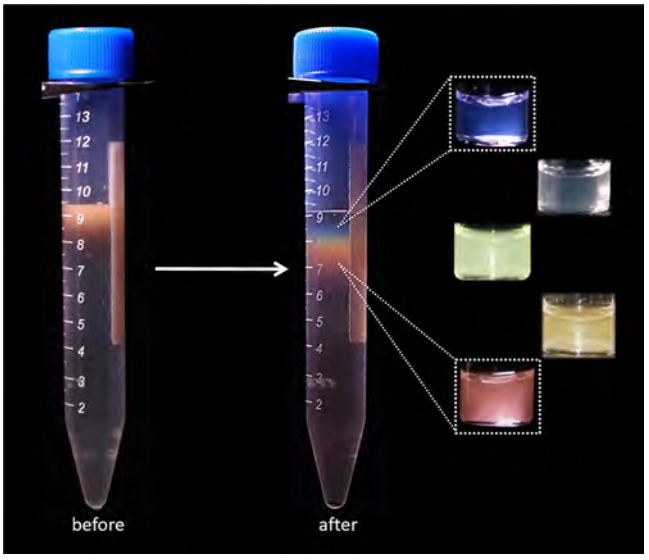

Figure 3. Density gradient separation. The tube is shown before and after centrifugation. The average diameters are calculated as 117 nm, PDI = 0.13 (blue); 124 nm, PDI = 0.17 (green); 140 nm, PDI = 0.059 (yellow); 160 nm, PDI = 0.053 (orange); and 240 nm, PDI = 0.054 (red).

For shape and size specification, we used scanning electron microscopy (SEM) and ImageJ software. The analysis showed that the obtained particles predominantly have a spherical shape (see Figure S5 of the Supporting Information). On the basis of more than 200 measurements of each color solution, average diameters are calculated as 117 ± 4, 124 ± 5, 140 ± 4, 160 ± 5, and 240 ± 6 nm. To estimate the distribution width, we calculated polydisersity indexes (PDIs). The resulting values were lower than 0.17, which indicates a moderate or high monodispersity (see Figure S5 of the Supporting Information) The data obtained are in accordance with dynamic light scattering (DLS) results, apart from some negligible errors (see Figure S4 of the Supporting Informa-

https://doi.org/10.1021/acs.langmuir.2c02382
Langmuir 2023, 39, 204−210

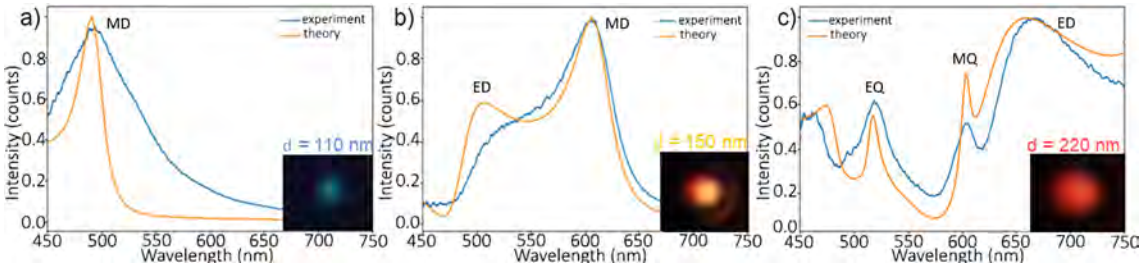

Figure 4. Comparison of theoretically modeled (orange curve) and experimentally obtained (blue curve) scattering spectra for the NPs with diameters of (a) 110 nm, (b) 150 nm, and (c) 220 nm and (insets) DF images of measured NPs.

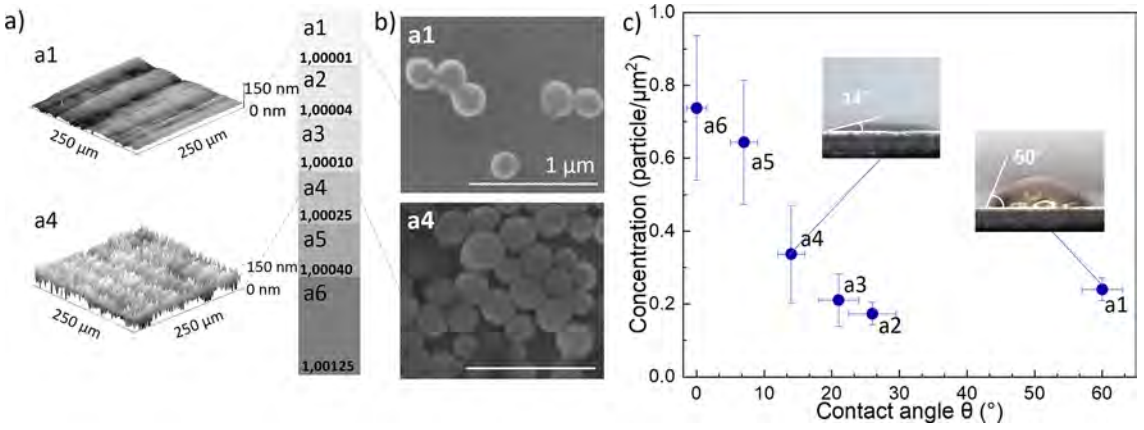

Figure 5. Wetting gradient on the steel surface for the controlled distribution of Si NPs: (a) scheme of a sample with a wetting gradient on the steel surface with the zones a1−a6, with the corresponding roughness value (profilograms of zones a1 and a4 are presented in the callout), (b) SEM images of Si NPs on laser-irradiated sample zones a1 and a4 (self-assembly of the Si NP monolayer can be seen on zone a4), and (c) dependence of the Si NP concentration on zones a1−a6 upon the contact angle.

tion). Then, we applied Raman spectroscopy to establish the phase composition of individual Si NPs. The narrow peak at 520 cm^{-1} confirms that individual NPs in different solutions are crystalline (see Figure S5 of the Supporting Information).

Mie Scattering of Si NPs. To predict the optical properties of the nanophotonic structures printed from the produced solutions and estimate the spherical shape of the NPs, we studied the light scattering from the individual Si NPs, both experimentally and numerically. For this purpose, we chose three typical NPs from different solutions placed on a glass substrate and illuminated by angularly incident light. The insets in Figure 4 represent the dark field (DF) optical images of these NPs. Different colors of NPs can be observed from DF images. Besides, the scattering spectra were measured from several individual NPs with uniform diameters and averaged. The experimental and numerically calculated spectra are shown in panels a−c of Figure 4.

Figure 4a shows the scattering signal from the NPs with a diameter of 110 nm. From both the experimental and numerically calculated spectra, a strong peak at the wavelength of 490 nm is observed, which corresponds to the magnetic dipole (MD) resonance according to the Mie theory.[31,32] For the NPs with a diameter of 150 nm (Figure 4b) this peak shifts to the wavelength of 605 nm, with the electric dipole (ED) resonance peak appearing at the wavelength of around 500 nm, while for the NP with a diameter of 220 nm (Figure 4c), there are also electric quadruple (EQ) and magnetic quadruple (MQ) modes appearing. To define peaks around 525 and 605 nm on the scattering spectra for the NPs with a diameter of 220 nm, we made multiple decomposition procedures, which show that that the peak at 605 nm corresponds to the magnetic quadruple resonance (MQ) and the peak at 525 nm corresponds to the electric quadruple (EQ) resonance. The experimental data are in good accordance with the numerical results, which confirms that the Si NPs obtained are spherical and crystalline.

Si NP Deposition over a Laser-Created Wetting Gradient on the Steel Surface. At the final step, we studied the influence of substrate wetting on the self-assembling process of Si NPs. For the experiments, we used the stainless-steel substrate as the model sample with controlled wettability. The wettability of this material is proven to be easily controlled by laser structuring in the air. The structuring modifies the metal roughness and produces metal oxides, thus changing the chemical composition, which modifies the hydrophility of the surface.[33,34] The degree of hydrophilicity in such a system can be estimated according to the Wenzel equation as

$$\cos \theta_r = r \cos \theta \quad (1)$$

where θ_r is the wetting angle on a rough surface, θ is the wetting angle on a smooth surface, and r is the roughness factor.

The test sample was produced by ns laser irradiation. It consists of six rectangular zones (a1−a6 in Figure 5a) with the size of 2 × 1 mm each (with the last zone of 2 × 2 mm). The laser irradiation was affected in the laser spot overlapping mode as 60%. The fluence was changed from 1.9 to 14.7 J/cm^2 to provide different wetting angles in the zones (see Figure S6 of the Supporting Information). The obtained wetting angles obtained for the NP solution are varied from 65° to 0° for a1−

https://doi.org/10.1021/acs.langmuir.2c02382
Langmuir 2023, 39, 204−210

a6, where the order of the zones is arranged with the wetting angles decreasing. When the solution droplet is applied to the most hydrophobic zone a1 of the gradient, the liquid spontaneously moves to a more hydrophilic zone a6. The liquid moves over the surface as a result of a decrease in the free surface energy of the laser structured surface. Figure 5a shows the obtained values of the roughness factor r (defined as the ratio of the actual surface area to its geometric surface area) of structured zones a1−a6.

Then, a drop of the water solution of Si NPs (volume of 0.1 μL) with an average diameter of 160 nm was applied to zone a1. The solution drop is spontaneously moving from a less hydrophilic zone (a1) to a more hydrophilic zone (a6); thus, the liquid flows directionally through the zones. The distributions of the Si NPs over the six zones with different wetting angles were studied by SEM (see Figure S7 of the Supporting Information).

As shown in the graph in Figure 5c, the concentration of the deposited NPs increases with a decrease in the contact angle, except for zone 1, where the concentration is slightly higher as a result of a higher surface tension of the liquid at the edge of the drop. We established that, starting from zone a4, the self-assembly of Si NPs is initiated on some parts of the zone (see examples in Figure 5b).

This effect can be explained by the changes in the solution zeta potential, capillary forces, and solution−surface contact time. When a NP solution droplet is applied to the wetting gradient, it spontaneously moves from the zone with a higher contact angle to the zone with a lower contact angle (more hydrophilic). Because the velocity of the dispersion medium increases compared to the dispersed phase during the drop movement, both the zeta potential and randomizing Brownian motion energy of the Si NP solution decrease. This initiates the coagulation of the Si NPs. At the same time, the capillary forces increase on the surface with a higher roughness (the most hydrophilic zone in the gradient). This effect provides additional attraction of Si NPs to each other and simultaneous concentration enhancement in the more hydrophilic zone. The impact of the capillary forces decreases during the solution evaporation, which is faster in the zones with higher contact angles. Another parameter influencing the Si NP concentration is the time of the solution−surface contact, which is higher for the zones with less contact angle. The combined effect of the zeta potential and Brownian motion decrease and the increase of the capillar forces as well as the solution/surface contact time provides a reduction of the Si interparticle distances. As a result, the role of van der Waals forces becomes more significant in the NP interaction. Therefore, the probability of the self-assembly process is higher in the zones with a smaller contact angle. Thus, the wetting control is utilized to manipulate interparticle interaction at the nanoscale for monolayer creation.

CONCLUSION

In our research, we described an approach for producing resonant Si NP colloidal solution with the PDI lower than 0.17 by ns laser ablation and a subsequent density gradient separation. We investigated the influence of the laser processing parameters on NP synthesis in DI water. We showed that λ = 1064 nm, f = 80 kHz, F = 4.38 J/cm^2, τ = 20 ns, and τ' = 10 s are the most preferable parameters for NP fabrication with the diameters from 100 to 200 nm. This optimization of laser ablation reduces material losses during the subsequent separation. The density gradient separation method in sucrose aqueous solutions was applied for post-processing the Si NP polydispersed colloid solution. Separation produced colloid solutions with the average Si NP diameters of 117 nm (blue), 124 nm (green), 140 nm (yellow), 160 nm (orange), and 240 nm (red). The PDI in solutions varied from 0.053 to 0.17. We also studied light scattering properties of the individual Si NPs obtained placed on the glass substrate. A comparison of the experimentally obtained and simulated scattering spectra appeared to be in a good accordance with the Mie theory, confirming experimentally obtained Si NPs being spherical and crystalline. To estimate the possibility of using the solutions obtained for self-assembly, the dielectric silicon NP solutions were spread by the drop casting over the substrates with a wetting gradient created by ns laser irradiation. We showed the effect of wetting the steel substrate on NP disposition. It was established that the concentration of deposited NPs increases with a decrease in the contact angle, which initiates the Si NP self-assembly on the zones with a concentration of over 0.3 particle/μm^2.

Thus, we proposed and verified the approach for the ns laser-assisted fabrication of colloidal solutions of resonant high-refractive index NPs and their self-assembly on the surface with a wetting gradient. All chemical procedures applied for the colloid nanofabrication are based on water and sucrose aqueous solution; therefore, the approach appears to be ecologically friendly. It can be prospectively extended for other transparent or flexible substrates. The result of the work seems to form the basis for applying Mie-resonant colloids for large-scale nanofabrication of metasurfaces and nanophotonic devices for various applications.

EXPERIMENTAL SECTION

Laser Processing. NP colloid solutions and wetting gradient are prepared using a setup based on a pulsed ytterbium fiber laser (Minimarker 2). The laser provides the following output parameters: the wavelength of λ = 1.064 μm, the pulses with a repetition rate of 1.6−99 kHz and pulse duration range of 4−200 ns, and the maximum average power of 20 W. The laser beam diameter in focus is 50 μm for NP fabrication and 13 μm for providing the wetting gradient.

NP fabrication experiments included several stages of material cleaning, generating NPs by a laser system, and optimization of laser ablation parameters based on SEM and DLS analyses. First, both the cuvette and target are cleaned in acetone, isopropyl alcohol, and DI water successively for 7 min at a temperature of 25 °C using an ultrasonic bath. Laser ablation is carried out in 800 mL (determined experimentally) of DI water inside the cleaned quartz cuvette. The parameters of laser ablation are given in Tables 1 and 2 of the Supporting Information. The size distribution of NPs was determined on the basis of the SEM images and presented by the statistics of particle diameters in Figures S2 and S3 of the Supporting Information. In our experimental conditions (laser fluence, scanning speed and scheme, pulses repetition rate, etc.), the laser ablation of the silicon target in DI water provides polydisperse Si NPs at the rate of 15 mL/h with the concentration value of approximately 10^{-3} M.

For the wetting gradient preparation, changes in the morphology and composition of the surface were produced by laser irradiation with the changing laser fluence F with a constant overlapping of laser pulse imprints $L_x = L_y$ = 60%. The average power of laser irradiation energy was measured using an energy and power meter "Gentec SoloPE-2". The structured zones of the steel surface were arranged in the order of the contact angle decreasing, creating a wetting gradient. For the laser formation of the wetting gradient on the surface, the rate is less than 20 s/cm^2, with the possibility of optimization using different scanning parameters (scanning speed, repetition rate, laser fluence, etc.).

https://doi.org/10.1021/acs.langmuir.2c02382
Langmuir 2023, 39, 204−210

Size Separation of Si NPs. The separation was conducted using a centrifuge SIGMA 3-16KL at 4000 rpm for 5 min. The density gradient was assisted with equal volumes of sucrose solutions containing 70, 50, 45, 40, 35 and 30% sucrose. They were prepared by dissolving sucrose in deionized water by sonication. For the experiments commercially available, the sucrose powder was purchased from the Lenreactiv company. The solutions of different concentrations were overlayered in a sequence, avoiding mixing, so that the density of these layers increased from 1.13 to 1.35 g/cm^3. A sample colloid solution was placed on a pre-formed linear gradient column after 10 min in ultrasonic bath Sapphire at the temperature of 25 °C.

Under centrifugal forces, the particles precipitated through the gradient column in separate zones, with each zone consisting of the NPs of a certain size and sedimentation rate. The layers were extracted from the top of the colorful gradient with an air displacement pipet and were replaced in different vials. To remove sucrose, the solutions were washed by 7 cycles of centrifugal sedimentation (10 000 rpm for 10 min, Microspin 12 centrifuge) and redispersing in DI water.

Numerical Simulation. A numerical simulation was carried out by the commercial software CST Studio Suite using the frequency domain solver. Si NPs were simulated as spheres made of crystalline silicon with the material parameters taken from ref 35 and with the diameters corresponding to the actual NP sizes. The NPs were placed on a glass substrate and illuminated by transverse electric (TE) and transverse magnetic (TM) polarized plane wave incident at an angle of 65° to the surface normal. The resulting signal is calculated as half of a sum of signals obtained under the incident TE and TM polarized light.

Characterization Techniques. *Geometry Characterization.* The geometry and size distribution of the NPs produced were analyzed by SEM (FEI). The NPs were deposited on a cleaned silicon bulk substrate. SEM imaging was performed via SEM FEI using the high voltage of 20 kV and the magnification of 1000−50 000 in a secondary electron detection mode. Analysis of the SEM images resulted in the size distributions obtained using both ImageJ software and Python script.

Phase Composition. The phase composition of the structures was investigated using Raman signal measurements. The spectra were recorded under normal aligned excitation of structures by a HeNe laser (HNL100LB, Thorlabs) with a wavelength of 632.8 nm and the output laser power of about 8 mW, which was focused on the structure surface by a Plan Apo, Mitutoyo 100× objective with numerical aperture (NA) = 0.7. The Raman signal was collected by the same objective into an ultraviolet−visible (UV−vis) Si detector [charge-coupled device (CCD), Andor DU 420A-OE 325] and recorded by Raman spectrometer Horiba LabRam HR800 with the diffraction grating of 1800 lines per millimeter.

DF Spectroscopy. The DF spectra of NPs were obtained under unpolarized light illumination from a halogen lamp (HL-2000-FHSA). The incident light at an angle of 65° to the surface normal was focused by a Plan Apo, Mitutoyo 10× objective with NA = 0.26, and the scattered signal from the NPs was collected from the normal to the surface direction by a Plan Apo, Mitutoyo 100× objective with NA = 0.7. The collected signal was recorded by Raman spectrometer Horiba LabRam HR800 with the diffraction grating of 150 lines per millimeter.

DLS. The Photocor complex was used as an express method to identify the size distribution of Si NPs fabricated in DI water. The equipment contains a thermally stabilized semiconductor laser (λ = 638 nm).

The hydrodynamic radius (R_h) and standard deviation (STD) were measured at a fixed scattering angle of 90°.

Wetting Gradient Characterization. The wetting angle was measured using a sessile drop method and a high-resolution ToupCam CCD camera. DI water and a colloidal solution of Si NPs with an average diameter of 160 nm were used as the test liquid. The drop volume for the measurements was 0.1 μL. The surface morphology was studied using SEM. Sample surface profilograms (with scanning step Z equal to 30 μm) were obtained with a ZeScope optical profilometer and processed using the Gwyddion software. The concentration of Si NPs distributed over the structured wetting surfaces was determined from SEM images and calculated using ImageJ software.

■ ASSOCIATED CONTENT

Supporting Information

The Supporting Information is available free of charge at https://pubs.acs.org/doi/10.1021/acs.langmuir.2c02382.

Influence of laser irradiation parameters, silicon NP characterization, and wetting experiments (PDF)

■ AUTHOR INFORMATION

Corresponding Authors

Galina Odintsova − *Institute of Laser Technologies, ITMO University, St. Petersburg 190031, Russia*; Email: gvodintsova@itmo.ru

Dmitry Zuev − *Department of Physics and Engineering, ITMO University, St. Petersburg 191002, Russia*; orcid.org/0000-0001-9157-5683; Email: d.zuev@metalab.ifmo.ru

Authors

Marina Karsakova − *Department of Physics and Engineering, ITMO University, St. Petersburg 191002, Russia*

Nadezhda Shchedrina − *Institute of Laser Technologies, ITMO University, St. Petersburg 190031, Russia*

Artur Karamyants − *Institute of Laser Technologies, ITMO University, St. Petersburg 190031, Russia*

Ekaterina Ponkratova − *Department of Physics and Engineering, ITMO University, St. Petersburg 191002, Russia*

Complete contact information is available at: https://pubs.acs.org/10.1021/acs.langmuir.2c02382

Notes

The authors declare no competing financial interest.

■ ACKNOWLEDGMENTS

Marina Karsakova, Nadezhda Shchedrina, Artur Karamyants, and Ekaterina Ponkratova are thankful to the School of Physics and Technology, ITMO University, for the support of laser NPs and wetting gradient fabrication on the surface substrate, SEM and optical studies of samples, and NP scattering spectra modeling. The works on separation of Si NPs by the density gradient method were supported by the Russian Science Foundation (21-72-30018).

■ REFERENCES

(1) Koshelev, K.; Kivshar, Y. Dielectric resonant metaphotonics. *ACS Photonics* **2021**, *8*, 102−112.

(2) Ma, Y.; Dong, B.; Lee, C. Progress of infrared guided-wave nanophotonic sensors and devices. *Nano Convergence* **2020**, *7*, 12.

(3) Oh, S.-H.; Altug, H.; Jin, X.; Low, T.; Koester, S. J.; Ivanov, A. P.; Edel, J. B.; Avouris, P.; Strano, M. S. Nanophotonic biosensors harnessing van der Waals materials. *Nat. Commun.* **2021**, *12*, 3824.

(4) Yesilkoy, F.; Arvelo, E. R.; Jahani, Y.; Liu, M.; Tittl, A.; Cevher, V.; Kivshar, Y.; Altug, H. Ultrasensitive hyperspectral imaging and biodetection enabled by dielectric metasurfaces. *Nat. Photonics* **2019**, *13*, 390−396.

(5) Kala, A.; Achanta, V. G. Dielectric encapsulations suitable for applications in quantum technologies. *Eur. Phys. J.: Spec. Top.* **2022**, *231*, 799−805.

(6) Johlin, E. Nanophotonic color splitters for high-efficiency imaging. *iScience* **2021**, *24*, 102268.
(7) Lin, Y.; Zheng, G.; Xin, Q.; Yuan, Q.; Zhao, Y.; Wang, S.; Wang, Z.-L.; Zhu, S.-N.; Jiang, C.; Song, A. Electrically Switchable and Flexible Color Displays Based on All-Dielectric Nanogratings. *ACS Appl. Nano Mater.* **2021**, *4*, 7182−7190.
(8) Kivshar, Y. All-dielectric meta-optics and non-linear nanophotonics. *Natl. Sci. Rev.* **2018**, *5*, 144−158.
(9) Grzelczak, M.; Liz-Marzán, L. M.; Klajn, R. Stimuli-responsive self-assembly of nanoparticles. *Chem. Soc. Rev.* **2019**, *48*, 1342−1361.
(10) Baranov, D. G.; Zuev, D. A.; Lepeshov, S. I.; Kotov, O. V.; Krasnok, A. E.; Evlyukhin, A. B.; Chichkov, B. N. All-dielectric nanophotonics: The quest for better materials and fabrication techniques. *Optica* **2017**, *4*, 814−825.
(11) Macfarlane, R. J. From Nano to Macro: Thinking Bigger in Nanoparticle Assembly. *Nano Lett.* **2021**, *21*, 7432−7434.
(12) Senyuk, B.; Meng, C.; Smalyukh, I. I. Design and preparation of nematic colloidal particles. *Langmuir* **2022**, *38*, 9099−9118.
(13) Rao, A.; Roy, S.; Jain, V.; Pillai, P. P. Nanoparticle Self-Assembly: From Design Principles to Complex Matter to Functional Materials. *ACS Appl. Mater. Interfaces* **2022**, DOI: 10.1021/acsami.2c05378.
(14) Zhang, Z.; Wang, H.; Su, M.; Sun, Y.; Tan, S.-J.; Ponkratova, E.; Zhao, M.; Wu, D.; Wang, K.; Pan, Q.; Chen, B.; Zuev, D.; Song, Y. Printed nanochain-based colorimetric assay for quantitative virus detection. *Angew. Chem.* **2021**, *133*, 24436−24442.
(15) Shao, R.; Meng, X.; Shi, Z.; Zhong, J.; Cai, Z.; Hu, J.; Wang, X.; Chen, G.; Gao, S.; Song, Y.; Ye, C. Marangoni Flow Manipulated Concentric Assembly of Cellulose Nanocrystals. *Small Methods* **2021**, *5*, 2100690.
(16) Szuwarzyński, M.; Mazur, Ł.; Borkowski, M.; Maćkosz, K.; Giżyński, K.; Mazur, T. Enhanced Assembly of Ag Nanoparticles for Surface-Independent Fabrication of Conductive Patterns. *ACS Appl. Nano Mater.* **2022**, *5*, 12711−12719.
(17) Chaâbani, W.; Proust, J.; Movsesyan, A.; Béal, J.; Baudrion, A.-L.; Adam, P.-M.; Chehaidar, A.; Plain, J. Large-scale and low-cost fabrication of silicon mie resonators. *ACS Nano* **2019**, *13*, 4199−4208.
(18) Okazaki, T.; Sugimoto, H.; Hinamoto, T.; Fujii, M. Color toning of Mie resonant silicon nanoparticle color inks. *ACS Appl. Mater. Interfaces* **2021**, *13*, 13613−13619.
(19) Sugimoto, H.; Okazaki, T.; Fujii, M. Mie resonator color inks of monodispersed and perfectly spherical crystalline silicon nanoparticles. *Adv. Opt. Mater.* **2020**, *8*, 2000033.
(20) Ionin, A.; Ivanova, A.; Khmel'nitskii, R.; Klevkov, Y.; Kudryashov, S.; Mel'nik, N.; Nastulyavichus, A.; Rudenko, A.; Saraeva, I.; Smirnov, N.; Zayarny, D.; Baranov, A.; Kirilenko, D.; Brunkov, P.; Shakhmin, A. Milligram-per-second femtosecond laser production of Se nanoparticle inks and ink-jet printing of nanophotonic 2D-patterns. *Appl. Surf. Sci.* **2018**, *436*, 662−669.
(21) Barcikowski, S.; Amendola, V.; Lau, M.; Marzun, G.; Rehbock, C.; Reichenberger, S.; Zhang, D.; Gökce, B.*Handbook of Laser Synthesis and Processing of Colloids*, 2nd ed.; DuEPublico: Essen, Germany, 2019.
(22) Kuzmin, P. G.; Shafeev, G. A.; Bukin, V. V.; Garnov, S. V.; Farcau, C.; Carles, R.; Warot-Fontrose, B.; Guieu, V.; Viau, G. J. Silicon nanoparticles produced by femtosecond laser ablation in ethanol: Size control, structural characterization, and optical properties. *J. Phys. Chem. C* **2010**, *114*, 15266−15273.
(23) Balling, P.; Schou, J. Femtosecond-laser ablation dynamics of dielectrics: Basics and applications for thin films. *Rep. Prog. Phys.* **2013**, *76*, 036502.
(24) Zhigunov, D. M.; Evlyukhin, A. B.; Shalin, A. S.; Zywietz, U.; Chichkov, B. N. Femtosecond laser printing of single Ge and SiGe nanoparticles with electric and magnetic optical resonances. *ACS Photonics* **2018**, *5*, 977−983.
(25) Shen, X.; Hsiao, P.-C.; Wang, Z.; Liu, M.; Phua, B.; Song, N.; Stokes, A.; Lennon, A. Modelling picosecond and nanosecond laser ablation for prediction of induced damage on textured SiN_x/Si surfaces of Si solar cells. *Prog. Photovoltaics* **2021**, *29*, 1020−1033.
(26) Chichkov, B. N.; Momma, C.; Nolte, S.; von Alvensleben, F.; Tünnermann, A. Femtosecond, picosecond and nanosecond laser ablation of solids. *Appl. Phys. A: Mater. Sci. Process.* **1996**, *63*, 109−115.
(27) Sundaram, S. K.; Mazur, E. Inducing and probing non-thermal transitions in semiconductors using femtosecond laser pulses. *Nat. Mater.* **2002**, *1*, 217−224.
(28) Zhang, D.; Gökce, B.; Barcikowski, S. Laser synthesis and processing of colloids: Fundamentals and applications. *Chem. Rev.* **2017**, *117*, 3990−4103.
(29) Kuznetsov, A. I.; Miroshnichenko, A. E.; Fu, Y. H.; Zhang, J.; Luk'yanchuk, B. Magnetic light. *Sci. Rep.* **2012**, *2*, 492.
(30) Sun, X.; Luo, L.; Kuang, Y.; Li, P.*Nanoseparation Using Density Gradient Ultracentrifugation: Mechanism, Methods and Applications*; Springer: Singapore, 2018; DOI: 10.1007/978-981-10-5190-6.
(31) Yan, J.; Liu, X.; Mao, B.; Yang, G.; Li, B. Individual Si Nanospheres Wrapped in a Suspended Monolayer WS_2 for Electromechanically Controlled Mie-Type Nanopixels. *Adv. Optical Mater.* **2021**, *9*, 2001954.
(32) Kuznetsov, A. I.; Miroshnichenko, A. E.; Brongersma, M. L.; Kivshar, Y. S.; Luk'yanchuk, B. Optically resonant dielectric nanostructures. *Science* **2016**, *354*, aag2472.
(33) Shchedrina, N.; Karlagina, Y.; Itina, T.; Ramos, A.; Correa, D.; Tokmacheva-Kolobova, A.; Manokhin, S.; Lutoshina, D.; Yatsuk, R.; Krylach, I.; Odintsova, G. Wetting angle stability of steel surface structures after laser treatment. *Opt. Quantum Electron.* **2020**, *52*, 163.
(34) Kietzig, A.-M.; Negar Mirvakili, M.; Kamal, S.; Englezos, P.; Hatzikiriakos, S. G. Laser-patterned super-hydrophobic pure metallic substrates: Cassie to Wenzel wetting transitions. *J. Adhes. Sci. Technol.* **2011**, *25*, 2789−2809.
(35) Green, M. A. Self-consistent optical parameters of intrinsic silicon at 300 K including temperature coefficients. *Sol. Energy Mater. Sol. Cells* **2008**, *92*, 1305−1310.

https://doi.org/10.1021/acs.langmuir.2c02382
Langmuir 2023, 39, 204−210